GEOPHYSICAL RESEARCH LETTERS, VOL. 34, L22317, doi:10.1029/2007GL031932, 2007

Empirical transfer functions: Application to determination of outermost core velocity structure using *SmKS* phases

Catherine Alexandrakis[1] and David W. Eaton[1]

Received 5 September 2007; revised 9 October 2007; accepted 19 October 2007; published 30 November 2007.

[1] *SmKS* waves provide good resolution of outer-core velocity structure, but are affected by heterogeneity in the D″ region. We have developed an Empirical Transfer Function (ETF) technique that transforms a reference pulse (here, *SmKS*) into a target waveform (*SKKS*) by: (1) time-windowing the respective pulses, (2) applying Wiener deconvolution, and (3) convolving the output with a Gaussian waveform. Common source and path effects are implicitly removed by this process. We combine ETFs from 446 broadband seismograms to produce a global stack, from which *S3KS-SKKS* differential time can be measured accurately. As a result of stacking, the scatter in our measurements (0.43 s) is much less than the 1.29 s scatter in previous compilations. Although our data do not uniquely constrain outermost core velocities, we show that the fit of most standard models can be improved by perturbing the outermost core velocity. Our best-fitting model is formed using IASP91 with PREM-like velocity at the top of the core. **Citation:** Alexandrakis, C., and D. W. Eaton (2007), Empirical transfer functions: Application to determination of outermost core velocity structure using *SmKS* phases, *Geophys. Res. Lett.*, *34*, L22317, doi:10.1029/2007GL031932.

1. Introduction

[2] Evidence from geodynamic [*Lister and Buffett*, 1998; *Buffett et al.*, 2000] and fluid immiscibility studies [*Helffrich and Kaneshima*, 2004] suggests that the outermost region of the Earth's core may contain one or more thin, low-density layers. Although such stratification is difficult to detect seismically, if present it could have a profound influence on the geodynamo [*Souriau and Poupinet*, 1991; *Lister and Buffett*, 1998; *Buffett et al.*, 2000].

[3] A number of previous studies have used teleseismic *SmKS* phases to improve seismic resolution in this region. *SmKS* waves (Figure 1) propagate as *S*-waves in the mantle and compressional (*K*) waves in the core, with $m - 1$ underside reflections from the core-mantle boundary (CMB). Since *SmKS* phases turn at relatively shallow depth beneath the CMB, they provide good resolution of outermost core velocity structure [*Choy*, 1977; *Garnero et al.*, 1993; *Tanaka*, 2004; *Eaton and Kendall*, 2006]. In particular, these waves comprise a whispering gallery phase [*Aki and Richards*, 1980] for which high-order ($3 \leq m < \infty$) modes coalesce into a composite, dispersive waveform at the range of periods for which they are typically observed (2–10 s).

[4] Most previous *SmKS* studies have focused on differential times between *SKS*, *SKKS* and *S3KS* phases, either using single-station techniques [*Souriau and Poupinet*, 1991; *Garnero et al.*, 1993; *Garnero and Helmberger*, 1995; *Souriau et al.*, 2003] or array techniques [*Tanaka*, 2004; *Eaton and Kendall*, 2006]. Under the assumption that source and mantle path effects are the same for each of these *SmKS* phases, differential times may be used to infer velocity structure of the outer core above the respective turning depths. Although significant differences exist between various proposed models, all previous studies indicate that seismic velocities of the outermost core are generally overestimated by PREM [*Souriau and Poupinet*, 1991; *Garnero et al.*, 1993; *Garnero and Helmberger*, 1995; *Souriau et al.*, 2003; *Tanaka*, 2004; *Tanaka*, 2007]. *Eaton and Kendall* [2006] found that a better fit is achieved for all models by inserting a thin (12 km) high-velocity, low-density layer near the top of the core.

[5] Global compilations of *SmKS* traveltime residuals along individual paths [*Souriau et al.*, 2003] exhibit a high degree of scatter, likely caused by lateral velocity variations in the D″ region [*Garnero et al.*, 1993]. *Tanaka* [2007] stacked long-period (T > 10s) waveforms to mitigate this effect, but due to source- and path-dependent waveform variability did not stack shorter period signals, thus sacrificing some fine-scale resolution of outer core structure. Here we introduce an Empirical Transfer Function (ETF) method that, like Receiver Functions [e.g., *Langston*, 1977; *Vinnik*, 1977], uses deconvolution to account for waveform differences and thus facilitates stacking of broadband waveforms. The purpose of this paper is to describe the ETF technique and to illustrate its application to the study of outermost core structure using *SmKS* differential time measurements.

2. *SmKS* Waves and Empirical Transfer Function Method

[6] The *SmKS* pulse contains a superposition of modes for $3 \leq m < \infty$ [*Choy*, 1977; *Eaton and Kendall*, 2006]. Relative to the preceding mode, each successive mode contains a time delay, phase shift and amplitude reduction. The phase shift arises from: (1) a Hilbert transform associated with the caustic at the turning point, (2) a small phase rotation, due to post-critical reflection from the base of the CMB, and (3) finite-frequency effects associated with the proximity of the turning point to the CMB [*Choy*, 1977]. While previous studies have usually incorporated the Hilbert transform [e.g., *Souriau et al.*, 2003; *Garnero et al.*, 1993; *Tanaka*, 2004], the remaining phase complications have generally been neglected. Here, we introduce ETF deconvolution as a way to simplify the analysis and inter-

[1]Department of Earth Sciences, University of Western Ontario, London, Ontario, Canada.

0094-8276/07/2007GL031932$05.00

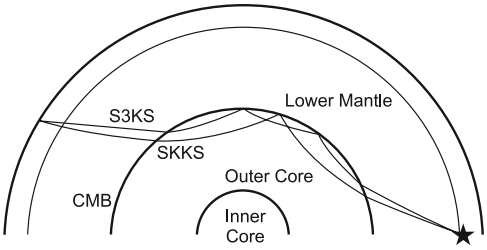

Figure 1. Ray geometry for *SKKS* and *S3KS*.

pretation of differential times between such closely related teleseismic phases. We define the ETF as a linear deconvolution operator that transforms a reference pulse (here, *SmKS*) into a target pulse (*SKKS*). By definition, the ETF incorporates all time shifts, phase rotations and amplitude changes associated with the modal summation process. We use a Wiener deconvolution approach to obtain the ETF, similar in principle to methods used in some surface-wave dispersion studies [e.g., *Taylor and Toksöz*, 1982] and receiver-function analyses [e.g., *Ai et al.*, 2003].

[7] Although the characteristics of *SmKS* waves are mainly sensitive to core velocity structure [*Choy*, 1977], properties of the D″ region can also influence the observed pulse. First, *SmKS* arrival time is sensitive to D″ velocity structure along both downgoing and upgoing paths. This is mitigated, however, by the use of differential times, since mantle paths for *SKKS* and *SmKS* ($m > 2$) phases are very similar [e.g., *Souriau and Poupinet*, 1991]. Here, residual traveltime anomalies are further reduced by stacking waveforms that sample different regions of the lower mantle. In addition, at each underside bounce point, the amplitude and phase of the reflection depends on local properties of both the core and the D″ region. Although pulse shape and amplitude are affected, underside CMB reflectivity will have only a minor (and indirect) influence on arrival times.

[8] As an initial step in the procedure, we isolate the *SKKS* and *SmKS* waveforms by time-windowing the input seismogram using a boxcar function with a Hanning taper at both ends (Figure 2). The start and end of the time window are event-specific parameters selected by the user, in much the same way that time windows are picked for shear-wave splitting analysis [e.g., *Silver and Chan*, 1991]. Adopting the terminology of Wiener filtering [*Wiener*, 1964], the Fourier-transformed *SmKS* and *SKKS* waveforms are here considered as the received and input signals, denoted by $U_m(\omega)$ and $U_2(\omega)$, respectively. These signals are related by a transfer function, $F(\omega)$, such that

$$U_m(\omega)F(\omega) = U_2(\omega). \tag{1}$$

Although $F(\omega)$ may be estimated directly by spectral division, this approach is typically unstable due to spectral holes in $U_m(\omega)$. A more stable solution may be obtained using Wiener deconvolution. For a given operator length in the time domain, Wiener deconvolution yields the function $\tilde{F}(\omega)$ that minimizes the least-squares difference between the left and right sides of equation (1). In the time domain, this function is obtained by solving a set of normal equations constructed using the cross-correlation of the two signals and the autocorrelation of the input signal [e.g., *Taylor and Toksöz*, 1982]. In the frequency domain, $\tilde{F}(\omega)$ may be expressed as

$$\tilde{F}(\omega) = \frac{C(\omega)}{A(\omega)} \tag{2}$$

where C and A are cross- and auto-spectra of the two signals, smoothed in accordance with the desired operator length [*Hwang and Mitchell*, 1986].

[9] Here, we define the ETF as the inverse Fourier transform of $\tilde{F}(\omega)$ and, for display purposes, convolve it with a Gaussian pulse

$$g(t) = \exp\left[-(t/T)^2\right]. \tag{3}$$

In practice, we find that a Gaussian pulse with a dominant period of $T \sim 5$ s is generally suitable, since it tends to suppress frequencies that are most affected by the windowing process.

[10] The procedure for measuring differential times using an ETF is illustrated in Figure 2. In the case where the received and input pulses are time-shifted and scaled but otherwise identical signals, the differential time is marked by a peak in the ETF. When the transfer function includes a phase shift, the differential time no longer corresponds to a peak but may still be extracted easily from the ETF. For example, in the case of a Hilbert transform, the differential time is marked by a zero crossing (Figure 2b), even if

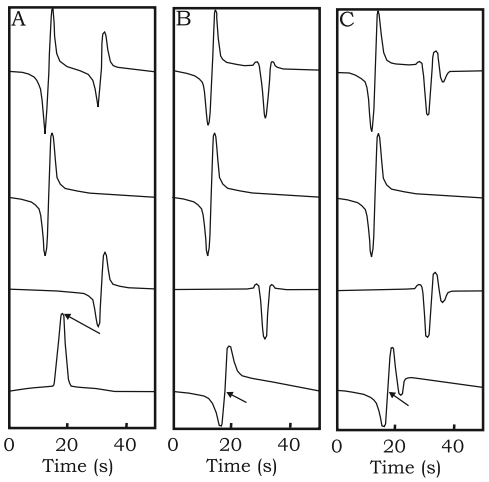

Figure 2. Illustration of ETF method. (a) Two signals of different amplitude (but otherwise identical) are separated by $\Delta t = 18.0$ s. The top trace shows the sum of both signals, the next two traces show the target and reference signals, respectively, and the bottom trace shows the computed ETF. The peak of the ETF (arrow) occurs at $t = \Delta t$. (b) As in Figure 2a, but the received signal is the Hilbert transform of the input signal, similar to the relationship of teleseismic *S3KS* to *SKKS*. Now the zero crossing of the ETF occurs at $t = \Delta t$. (c) As in Figure 2b, but the top trace contains a third signal with a delay of 22.0 s after the input signal. Two Hilbert transforms have been applied to the third signal, similar to the relationship of teleseismic *S4KS* to *SKKS*. The ETF is more complex, but the first zero crossing still occurs at $t = \Delta t$.

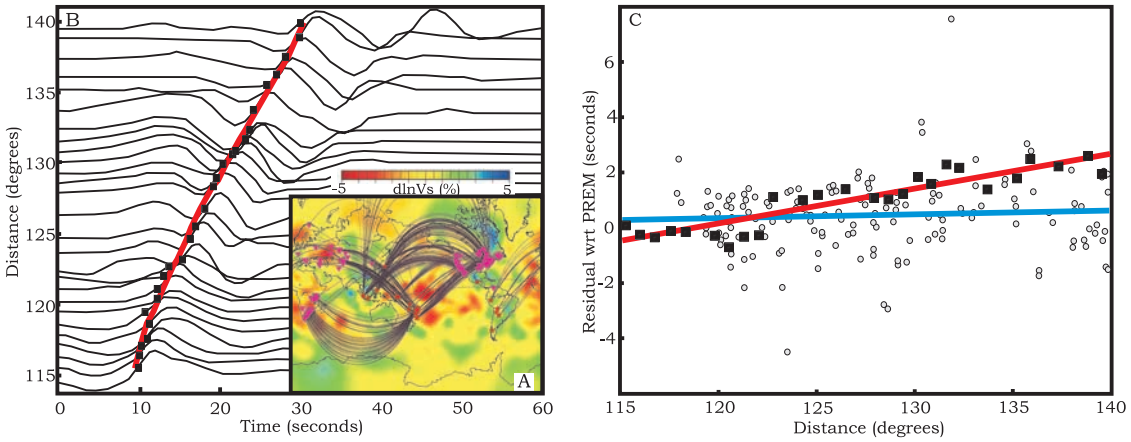

Figure 3. (a) Events (stars) and stations (inverted triangles) used in this study, with corresponding raypaths, superimposed on map of shear-wave velocity perturbation of the D″ region (2850 km depth) in %, from model SAW24B16 [*Mégnin and Romanowicz*, 2000]. (b) Stacked ETF record section with zero crossing picks corresponding to the *S3KS-SKKS* differential time. Inferred moveout curve is indicated. (c) Graph of *S3KS-SKKS* differential time residuals with respect to PREM. Single station data [from *Souriau et al.*, 2003] are shown by circles, data from this study are shown by squares. We converted *SKKS* ray parameter to epicentral distance using a reference focal depth of 500 km. The RMS residuals with respect to the two lines of best fit for the single station observations and this study's observations are 1.29 s (dashed line) and 0.43 s (solid line), respectively.

additional phases are present (Figure 2c). The majority of previously reported single-station *SmKS* differential times have been measured by cross-correlating the seismogram with its Hilbert transform or with a synthetic seismogram. Since Wiener deconvolution is also based on cross-correlating the two waveforms, picking the zero crossing of an ETF yields an equivalent proxy measurement of differential time. We remark that, for the purpose of determining differential time using a single seismogram, the ETF procedure offers no advantage over cross-correlation methods. The advantage comes, rather, from the ability to stack deconvolved broadband waveforms from different events prior to the determination of differential time, since a waveform-stacking approach is generally more robust than averaging of individual measurements.

[11] As noted above, full-waveform theory [*Choy*, 1977] shows that the transfer function between successive *SmKS* pulses includes other phase shifts in addition to the 90° phase shift from the Hilbert transform. To account for these effects, we compared our results with ETFs obtained from synthetic seismograms computed using the reflectivity method [*Fuchs and Müller*, 1971], which includes contributions from the complete *SmKS* series.

3. Results

[12] We computed ETFs for 446 radial-component broadband seismograms containing high-quality *SmKS* observations during the time period 1994–2007. We confined our observations to a distance range of 115–140°, within which the mean turning depth of *SKKS* and *S3KS* lies in the top 350 km of the core, where global velocity models exhibit the greatest variability [*Eaton and Kendall*, 2006]. To the extent possible, broadband seismograms with coherent *SmKS* phases were selected to include paths that sample high and low-velocity regions of the lowermost mantle, in an attempt to average out the effects of D″ heterogeneity (Figure 3a). We sorted ETFs into bins according to *SKKS* ray parameter, discarded bins containing 4 or fewer traces, and stacked the results to create a global record section (Figure 3b). Our interpretation of the stacked ETF record section assumes that the outer core is much more homogeneous than the lowermost mantle [e.g., *Souriau et al.*, 2003]. This implies that by stacking a sufficient number of observations, perturbations caused by lower mantle heterogeneity will tend to average out.

[13] *S3KS-SKKS* differential times were obtained by measuring the corresponding zero crossings. To estimate a *S3KS-SKKS* differential time function (moveout curve), we computed residual times with respect to the model PREM [*Dziewonski and Anderson*, 1981] and performed a least-squares linear regression with respect to epicentral distance (Figure 3c). The root-mean-squared (RMS) difference between our measurements and the line of best fit is 0.43 s, compared to a 1.29 s RMS scatter for previously compiled single-station measurements [*Souriau et al.*, 2003] within the same range of epicentral distance. Our data exhibit a trend of increasing residual with distance, a trend also noted by *Souriau et al.* [2003], albeit with a smaller slope. The positive time residuals are consistent with lower velocities in the outer part of the core, relative to PREM, found in other standard Earth models [*Eaton and Kendall*, 2006].

[14] Since any realistic radially symmetric Earth model predicts a smoothly varying *S3KS-SKKS* differential time function, we assumed that the scatter in our measured arrival times results from heterogeneous Earth structure, especially in the D″ region, which is not entirely averaged out by the stacking process. We used the regression line to obtain an inferred moveout curve, by adding it to the predicted differential times from PREM. This *S3KS-SKKS* moveout curve provides a new kinematic constraint against which velocity models for the core may be tested. To search the parameter space in the neighborhood of existing standard Earth models (which satisfy many other constraints

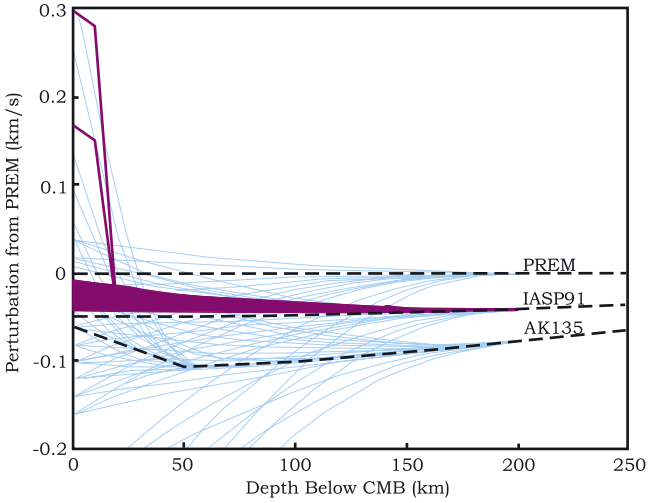

Figure 4. Summary of velocity models that fit our observed *S3KS-SKKS* differential time, plotted as difference from PREM. Trial models (thin lines) were created by perturbing standard Earth models PREM, IASP91, and AK135. Note that PREM, IASP91, and AK135 (dashed lines) do not fit the data, but are shown here for reference. The filled area indicates the range of velocity models that fit our observations. Two models that included a high velocity layer at the top of the core (thick lines), as described by *Helffrich and Kaneshima* [2004], were tested and found to be acceptable.

beyond those considered here), we constructed trial velocity models by perturbing the models PREM [*Dziewonski and Anderson*, 1981], IASP91 [*Kennett and Engdahl*, 1991] and AK135 [*Kennett et al.*, 1995]. Trial models were created by: (1) assigning a *P*-wave velocity, *Vp* to the top of the core; (2) requiring *Vp* to be continuous with the starting model at 200 km depth below the CMB; and (3) using a quadratic function to smoothly join the top of the core with the velocity at depth. We sampled a *Vp* range at the CMB of 7.7 – 8.4 km/s, sampling every ~0.02 km/s (Figure 4). To evaluate the acceptability of each trial model, we computed synthetic seismograms using the reflectivity method [*Fuchs and Müller*, 1971], used the synthetic traces to construct an ETF record section, measured the zero-crossing times and computed the RMS difference with respect to our moveout curve.

[15] In cases where the RMS misfit between the modeled times and the moveout curve exceeded the observed scatter (0.43 s), we deemed a trial Earth model to be unacceptable. Using this criterion, we found that PREM, IASP91 and AK135 (RMS misfit of 0.48 s, 0.52 s and 0.49 s, respectively) are all marginally unacceptable. Slight perturbations to IASP91 using our simple search strategy yielded models that fit our acceptance criterion (Figure 4). Of all models tested, the one with the lowest RMS misfit (0.27 s) used IASP91 as a base model, with a PREM-like velocity of 8.040 km/s at the top of the core. Relative to PREM, this model contains a velocity "sag" in the outer 200 km of the core, consistent with the conclusions of most previous studies of *SmKS* [*Souriau and Poupinet*, 1991; *Garnero et al.*, 1993; *Garnero and Helmberger*, 1995; *Souriau et al.*, 2003; *Tanaka*, 2004; *Eaton and Kendall*, 2006; *Tanaka*, 2007].

[16] We also considered whether models containing a thin, high-velocity layer beneath the CMB can be excluded based on our kinematic criteria. To evaluate this possibility, we superimposed a constant-velocity layer 10 km thick at the top of our best fitting model, and tested velocities of 8.23 and 8.36 km/s. These velocity values correspond with possible values for a light *S*-rich, immiscible fluid layer proposed by *Helffrich and Kaneshima* [2004] for core temperatures of 3500 and 4300 K, respectively. Although the addition of such a layer increases the misfit from the best-fitting model, these two models still meet our acceptance criteria since the misfit (0.28 s and 0.30 s) is still below the scatter in the observed data.

4. Conclusions

[17] The Empirical Transfer Function method proposed here is a new method for measuring the differential time between a reference phase (in this case, *SmKS*) and a target phase (*SKKS*) that facilitates stacking of waveforms from different paths. Using this method, we have constructed a global stacked record section, from which the *S3KS-SKKS* differential time can be measured directly. This approach yields significantly less scatter (0.43 s) than previous single-station and array-analysis methods (1.29 s). By perturbing standard Earth models, we have identified a range of velocity models that fit the observed data to within the scatter in our observations. Our best fitting model is derived from IASP91, but has a PREM-like velocity at the top of the core. On the basis of our results, we cannot rule out the possibility of a thin, high velocity layer at the top of the core as proposed by *Helffrich and Kaneshima* [2004] and *Eaton and Kendall* [2006]. As more data becomes available, the stacked global reference section should improve, resulting in less scatter. When sufficient data becomes available, this should provide a strong constraint on the velocity structure of the outermost core.

[18] **Acknowledgments.** The authors are grateful to S. Tanaka, who provided a preprint of his 2007 manuscript. GMT software [*Wessel and Smith*, 1998] was used to produce parts of Figure 3. This work was funded by the Natural Sciences and Engineering Research Council of Canada and by an Ontario Graduate Scholarship in Science and Technology to C.A. Data used for this study were obtained from the waveform archives of IRIS and POLARIS.

References

Ai, Y., T. Zheng, W. Xu, Y. He, and D. Dong (2003), A complex 660 km discontinuity beneath northeast China, *Earth Planet. Sci. Lett.*, *212*, 63–71.

Aki, K., and P. G. Richards (1980), *Qualitative Seismology: Theory and Methods*, W. H. Freeman, San Francisco, Calif.

Buffett, B. A., E. J. Garnero, and R. Jeanloz (2000), Sediments at the top of Earth's core, *Science*, *290*, 1338–1342.

Choy, G. (1977), Theoretical seismograms of core phases calculated by frequency-dependent full wave theory, and their interpretation, *Geophys. J. R. Astron. Soc.*, *51*, 275–312.

Dziewonski, A. M., and D. L. Anderson (1981), Preliminary reference Earth model, *Phys. Earth Planet. Inter.*, *25*, 297–356.

Eaton, D. W., and J. M. Kendall (2006), Improving seismic resolution of outermost core structure by mulitchannel analysis and deconvolution of broadband *SmKS* phases, *Phys. Earth Planet. Inter.*, *155*, 104–119.

Fuchs, K., and G. Müller (1971), Computation of synthetic seismograms with the reflectivity method and comparison with observations, *Geophys. J. R. Astron. Soc.*, *23*, 417–433.

Garnero, E. J., and D. V. Helmberger (1995), On seismic resolution of lateral heterogeneity in the Earth's outermost core, *Phys. Earth Planet. Inter.*, *88*, 117–130.

Garnero, E. J., D. V. Helmberger, and S. P. Grand (1993), Constraining outermost core velocity with *SmKS* waves, *Geophys. Res. Lett.*, *20*(22), 2463–2466.

Helffrich, G., and S. Kaneshima (2004), Seismological constraints on core composition from Fe-O-S liquid immiscibility, *Science*, *306*, 2239–2242.

Hwang, H. J., and B. J. Mitchell (1986), Interstation surface wave analysis by frequency-domain wiener deconvolution and modal isolation, *Bull. Seismol. Soc. Am.*, *76*, 847–864.

Kennett, B. L. N., and E. R. Engdahl (1991), Traveltimes for global earthquake location and phase identification, *Geophys. J. Int.*, *105*, 429–465.

Kennett, B. L. N., E. R. Engdahl, and R. Buland (1995), Constraints on seismic velocities in the Earth from traveltimes, *Geophys. J. Int.*, *122*, 108–124.

Langston, C. A. (1977), Corvallis, Oregon, crustal and upper mantle structure from teleseismic P and S waves, *Bull. Seismol. Soc. Am.*, *67*, 713–724.

Lister, J. R., and B. A. Buffett (1998), Stratification of the outer core at the core-mantle boundary, *Phys. Earth Planet. Inter.*, *105*, 5–19.

Mégnin, C., and B. Romanowicz (2000), The shear velocity structure of the mantle from the inversion of body, surface and higher mode waveforms, *Geophys. J. Int.*, *143*, 709–728.

Silver, P. G., and W. W. Chan (1991), Shear wave splitting and subcontinental mantle deformation, *J. Geophys. Res.*, *96*(B10), 16,429–16,454.

Souriau, A., and G. Poupinet (1991), A study of the outermost liquid core using differential travel times of the SKS, SKKS and S3KS phases, *Phys. Earth Planet. Inter.*, *68*, 183–199.

Souriau, A., A. Teste, and S. Chevrot (2003), Is there any structure inside the liquid outer core?, *Geophys. Res. Lett.*, *30*(11), 1567, doi:10.1029/2003GL017008.

Tanaka, S. (2004), Seismic detectability of anomalous structure at the top of the Earth's outer core with broadband array analysis of *SmKS* phases, *Phys. Earth Planet. Inter.*, *141*, 141–152.

Tanaka, S. (2007), Possibility of a low *P*-wave velocity layer in the outermost core from global *SmKS* waveforms, *Earth Planet. Sci. Lett.*, *259*, 486–499.

Taylor, S. R., and M. N. Toksöz (1982), Measurement of interstation phase and group velocities and *Q* using Wiener Filtering, *Bull. Seismol. Soc. Am.*, *72*, 73–91.

Vinnik, L. P. (1977), Detection of waves converted from P to SV in the mantle, *Phys. Earth Planet. Inter.*, *15*, 39–45.

Wessel, P., and W. H. F. Smith (1998), New, improved version of the Generic Mapping Tools released, *Eos Trans. AGU*, *79*, 579.

Wiener, N. (1964), *Extrapolation, Interpolation, and Smoothing of Stationary Time Series With Engineering Applications*, 163 pp., MIT Press, Cambridge, Mass.

C. Alexandrakis and D. W. Eaton, Department of Earth Sciences, University of Western Ontario, 1151 Richmond Street, London, ON, Canada N6A 5B7. (calexan3@uwo.ca)